RSC Advances

PAPER

View Article Online
View Journal | View Issue

Check for updates

Cite this: *RSC Adv.*, 2026, **16**, 24141

Acceptor-driven synergy in dihydropyridine-based compounds reveals giant static and frequency-dependent hyperpolarizabilities: a quantum exploration

Khansa Gull,[a] Memoona Arshad,[a] Sadia Jamal,[a] Rifat Jawaria,[*a] Saif Ullah[b] and Muhammad Imran[cd]

Dihydropyridine carbonitrile derivatives exhibit strong nonlinear optical (NLO) performance due to efficient charge-transfer properties, making them promising for optical applications. In current study, dihydropyridine carbonitrile based compounds (**CTP1–CTP6**) were designed by structural modeling of reference compound (CTPR) with malononitrile-based acceptors for utilization as NLO materials. All quantum chemical calculations were performed *via* DFT and TD-DFT methods at the M06/6-311G(d,p) level of theory. The designed molecules have donor–π–acceptor (D–π–A) framework, and this push–pull archiecture was improved by the introduction of electron-withdrawing moiety on acceptors. FMO analysis revealed small energy gaps and effective charge transfer from donor to acceptor regions. The absorbance maxima varied from 412 to 584 nm, indicating a redshift in optical behavior. The significant NLO properties were investigated in **CTP4**, including average polarizability (1.443×10^{-22} esu), first-order hyperpolarizability (9.279×10^{-28} esu), and second hyperpolarizability (4.231×10^{-33} esu), owing to its good optoelectronic properties. The first hyperpolarizability shows a remarkable enhancement, with a maximum value of 9.279×10^{-28} esu (**CTP4**), which is nearly 10^2–10^3 times higher than that of *para*-nitroaniline (*p*-NA), the standard reference compound. These findings qualitatively indicate that structural modification can greatly enhance the charge-transfer efficiency and quantitatively make the studied systems promising for high-performance optoelectronic and photonic applications.

Received 19th December 2025
Accepted 8th April 2026

DOI: 10.1039/d5ra09811d

rsc.li/rsc-advances

Open Access Article. Published on 08 May 2026. Downloaded on 5/10/2026 4:06:46 PM.
This article is licensed under a Creative Commons Attribution-NonCommercial 3.0 Unported Licence.

Introduction

The NLO is a growing branch in contemporary optics that deals with the effects of powerful electromagnetic radiation on matter, specifically producing an array of nonlinear effects.[1,2] When matter exposed to intense laser fields, the optical responses of a material will not only be modified but may also produce new light frequencies and improve optoelectronic properties.[3] Second-order NLO materials have shown widespread application in optical communication, photonic switching, biosensing, imaging and optical limiting because of their large nonlinear responses.[4] Recent attempts to model new NLO-active systems have been focused on organic and inorganic semiconductors, polymers, nanomaterials and molecular dyes.[5–7] Among these, organic materials are particularly interesting because of their large polarizability and molecular flexibility as well as their good charge-transport characteristics.[8] The NLO responses of a given species are mostly determined by its linear polarizability (α), second-order hyperpolarizability (β) and third-order hyperpolarizability (γ).[9–13] The second and third NLO orders play important roles in the SHG for device applications such as electro-optical modulation, high-speed optical switching and data processing.[14] Molecular systems with extended π-conjugation exhibit remarkable NLO responses, primarily driven by efficient intramolecular charge transfer (ICT) from the electron-donating (D) to electron-accepting (A) groups through π-linkers. Reported studies highlight various structurally engineered frameworks, such as donor–acceptor, donor–π–acceptor, donor–π–acceptor–π–donor, donor–π–π–acceptor, and donor–acceptor–π–acceptor, that have been tailored to enhance charge delocalization and NLO response.[15–18]

In the present investigation, a series of dihydropyridine-based systems with a donor–π–acceptor (D–π–A) configuration were designed in order to evaluate their potential NLO-activities. The π-spacer is the key structural unit that determines the degree of electronic delocalization and charge

[a]*Institute of Chemistry, Khwaja Fareed University of Engineering & Information Technology, Rahim Yar Khan, 64200, Pakistan. E-mail: rifat.jawaria@kfueit.edu.pk*
[b]*Govt Sadiq Abbas Graduate College Dera Nawab Sahib, Pakistan*
[c]*Department of Chemistry, Faculty of Science, King Khalid University, P.O. Box 9004, Abha 61413, Saudi Arabia*
[d]*Research Center for Advanced Materials Science (RCAMS), King Khalid University, P. O. Box 9004, Abha 61514, Saudi Arabia*

© 2026 The Author(s). Published by the Royal Society of Chemistry

Open Access Article. Published on 08 May 2026. Downloaded on 5/10/2026 4:06:46 PM. This article is licensed under a Creative Commons Attribution-NonCommercial 3.0 Unported Licence.

transfer across the molecule. This study primarily focuses on evaluating the NLO response of 2-oxo-6-thiophen-2-yl-1,2-dihydro-pyridine-3-carbonitrile derivatives. The study is based on the findings of Vishrutha *et al.*, who described the synthesis of 4-(9-methyl-9*H*-carbazol-3-yl)-2-oxo-6-thiophen-2-yl-1,2-dihydro-pyridine-3-carbonitrile,[19] a non-fullerene chromophore with superior optoelectronic properties. Here, the study has been expanded using computational modeling of the NLO parameters together with nonlinear optical data analysis in order to further elucidate the NLO properties of this family of compounds. The structural motif, 9,9′-bifluorenylidene, is a framework in which two fluorene entities are bonded through a single bond, endowing it with flexible conjugation. Similarly, the 2-oxo-6-thiophen-2-yl-1,2-dihydro-pyridine-3-carbonitrile spacer facilitates efficient charge migration from the donor to the acceptor region, enhancing ICT. The 9-methyl-9*H*-carbazole moiety acts as a strong electron-donating fragment, imparting stability and favorable optoelectronic characteristics to the designed molecules. Malononitrile-based acceptors are extensively utilized in the construction of organic optoelectronic materials since they possess high electron-withdrawing ability and superior conjugation with π-systems. Cyano (–CN) groups on the malononitrile moiety significantly enhance the electron-accepting power of the molecule, allowing efficient ICT in push–pull architectures. Given these properties, malononitrile derivatives have found wide use in the preparation of high-performance materials in NLO and other photonic devices.[20,21] Herein, these malononitrile-based acceptors were utilized to design **CTP1–CTP6** chromophores for NLO applications. Their optoelectronic properties were explored through DFT/TD-DFT methodologies, and, based on the results, it is anticipated that these chromophores will be reasonable candidates for optical devices.

Computational procedure

Density functional theory (DFT) and time-dependent density functional theory (TD-DFT) investigations were executed using the Gaussian 16 package.[22] Initially, the M06 functional[23] and 6-311G(d,p) basis set were utilized for optimization of the frequency calculations for all the derivatives (**CTPR** and **CTP1–CTP6**). The absence of negative frequencies confirmed the stability of the optimized structures. By utilizing these optimized structures, different analyses, such as absorption properties (UV-Vis), frontier molecular orbital (FMOs), transition density matrix (TDM), and electron hole investigations, were conducted in order to investigate the electrical and optical characteristics of the entitled chromophores. The NLO properties were investigated with the M06 functional along with the diffuse basis set 6-311G+(d,p). Various software packages were used to extract information from the Gaussian output files. Avogadro software[24] was used to generate the FMO diagrams, HOMO–LUMO orbitals and their corresponding energies. PyMOlyze 1.1 program[25] was used to interpret the orbital composition spectrum of the designed molecules. The UV-Visible data were extracted using GaussSum,[26] and graphs were generated using Origin 8.5 software.[27] Moreover, the natural bond orbitals (NBOs) study, to ascertain the stability pattern of the designed compounds, was conducted using the NBO 7 program.[28] The values of the dipole moment (μ^D),[29] linear polarizability $\langle\alpha\rangle$,[30] first-order hyperpolarizability (β_{total}), and second-order hyperpolarizability (γ_{total})[31] were calculated using eqn (1)–(4).

$$\mu^D = (\mu_x^2 + \mu_y^2 + \mu_z^2)^{1/2} \quad (1)$$

$$\langle\alpha\rangle = (a_{xx} + a_{yy} + a_{zz})^{1/3} \quad (2)$$

$$\beta_{total} = (\beta_x^2 + \beta_y^2 + \beta_z^2)^{1/2} \quad (3)$$

where $\beta_x = \beta_{xxx} + \beta_{xyy} + \beta_{xzz}$, $\beta_y = \beta_{yyy} + \beta_{xxy} + \beta_{yzz}$, and $\beta_z = \beta_{zzz} + \beta_{xxz} + \beta_{yyz}$

$$\langle\gamma\rangle = \sqrt{\gamma_x^2 + \gamma_y^2 + \gamma_z^2} \quad (4)$$

where, $\gamma_i = \frac{1}{15}\sum_j(\gamma_{ijji} + \gamma_{ijij} + \gamma_{iijj}) \quad i,j = \{x,y,z\}$.

The frequency-dependent NLO responses calculated in this study correspond to various photonic phenomena, including second-harmonic generation (SHG), third-harmonic generation (THG), the electro-optic pockels effect (EOPE), and the electro-optic Kerr effect (EOKE). In particular, SHG arises from the first-order hyperpolarizability term $\beta(-2\omega;\ \omega,\ \omega)$, THG is determined by the second-order hyperpolarizability $\gamma(-2\omega;\ \omega,\ \omega,\ \omega)$, EOPE corresponds to $\beta(-\omega;\ \omega,\ 0)$, while EOKE is described by $\gamma(-\omega;\ \omega,\ 0,\ 0)$. These dynamic first hyperpolarizability can be represented by the following equation

$$\beta(\omega) = [(\beta_x^2 + \beta_y^2 + \beta_z^2)]^{1/2} \quad (5)$$

The second harmonic generation (SHG) coefficients are calculated using the following equation

$$\beta_i = \beta_{iii}(-2\omega,\ \omega,\ \omega) + \beta_{ijj}(-2\omega,\ \omega,\ \omega) + \beta_{ikk}(-2\omega,\ \omega,\ \omega) \quad (6)$$

The electro-optical Pockels effect (EOPE) coefficients are calculated by following equation

$$\beta_i = \beta_{iii}(-\omega,\ \omega,\ 0) + \beta_{ijj}(-\omega,\ \omega,\ 0) + \beta_{ikk}(-\omega,\ \omega,\ 0) \quad (7)$$

The frequency-dependent second-order hyperpolarizability is calculated as follows

$$\gamma(\omega) = \sqrt{\gamma_x^2(\omega) + \gamma_y^2(\omega) + \gamma_z^2(\omega)} \quad (8)$$

Results and discussion

In the current research, the electronic and nonlinear optical properties of the proposed compounds were studied to investigate their potential applications in optoelectronic devices. The reference compound, **CTPR**, and six dihydro-pyridine based compounds **CTP1–CTP6**, with D–π–A configuration, were designed by substituting different effective acceptor groups: 2-(6-fluoro-2-methylene-3-oxo-indan-1-ylidene)-malononitrile as

© 2026 The Author(s). Published by the Royal Society of Chemistry

Open Access Article. Published on 08 May 2026. Downloaded on 5/10/2026 4:06:46 PM.
This article is licensed under a Creative Commons Attribution-NonCommercial 3.0 Unported Licence.

A1, 2-(5,6-difluoro-2-methylene-3-oxo-indan-1-ylidene)-malononitrile as A2, 2-(5,6-dichloro-2-methylene-3-oxo-indan-1-ylidene)-malononitrile as A3, 1-dicyanomethylene-3-oxo-indan-5,6-dicarbonitrile as A4, 2-(2-methylene-5,6-dinitro-3-oxo-indan-1-ylidene)-malononitrile as A5 and 2-(2-methylene-3-oxo-5,6-bis-trifluoromethyl-indan-1-ylidene)-malononitrile as A6, as reported in the literature.[32] In all derivatives (**CTP1–CTP6**), different acceptor species were used while the donor moiety was retained. Fig. 1 illustrates the structural tailoring of the compounds. ChemDraw structures of all the studied chromophores are shown in Fig. S1, while their optimized geometries are shown in Fig. 2. Table S1 lists the IUPAC names of **CTP1–CTP6** compounds. Tables S2–S8 show the Cartesian coordinates of all compounds.

The D–π–A framework was adopted to enhance the optoelectronic and NLO properties of the designed compounds. This study aims to evaluate their NLO performance and potential for optoelectronic applications. The influence of different electron-withdrawing groups was explored by modifying the acceptor units. Quantum chemical analyses were performed using DFT/TD-DFT (M06/6-311G(d,p)) to assess energy gaps (E_g), UV-visible absorption (λ_{max}), global reactivity parameters (GRPs), binding energies (E_b), and NLO parameters ($\langle\alpha\rangle$, μ_{total}, β_{total}, γ_{total}). The results provide valuable insights for future experimental synthesis and the development of efficient NLO materials.

Planarity parameters

To evaluate how the π-spacer affects the overall planarity of the π-conjugated frameworks, Multiwfn[33] was used to determine the molecular planarity parameter (MPP) and span of deviation (SDP) from the plane. The MPP estimates the structure's overall deviation from the plane, whereas SDP indicates the divergence of individual sections from planarity.[34] The structure will be more planar if MPP and SDP are lower, which ultimately leads to improved conjugation across the structure. In addition, the estimated maximal positive deviation (MPD) and maximal negative deviation (MND) from the fitted plane gave an indication of which atoms in the whole structure deviated from the plane most. All of these parameters are displayed in Table 1.

The MPP values of all the designed compounds (**CTPR–CTP6**) fall between 0.525 and 1.395 Å, indicating the compounds have generally planar structures. Among all compounds, **CTP1** and **CTP2** have the lowest MPP values, showing that their structures are planar, and their balanced MPD and MND values support the conclusion that these derivatives almost lie in one plane. This enhanced planarity

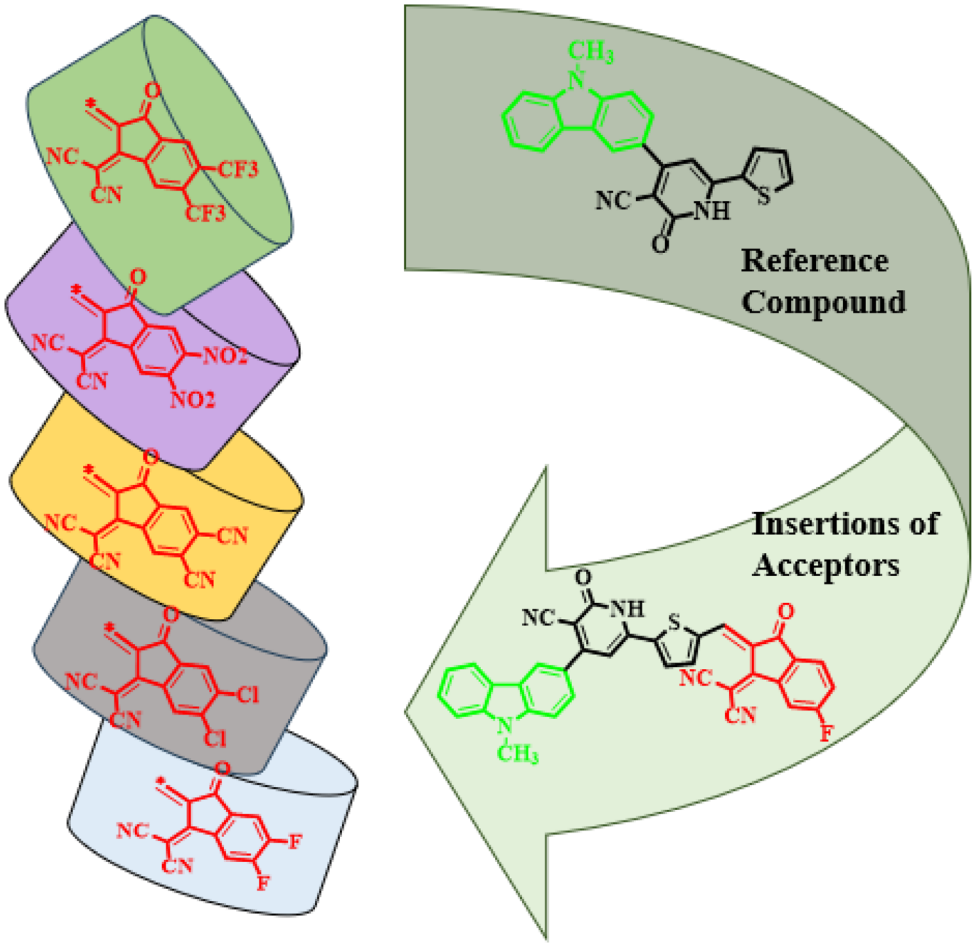

Fig. 1 Graphical representation of the design of CTPR–CTP6 chromophores by utilizing various malononitrile-based acceptors.

Open Access Article. Published on 08 May 2026. Downloaded on 5/10/2026 4:06:46 PM.
This article is licensed under a Creative Commons Attribution-NonCommercial 3.0 Unported Licence.

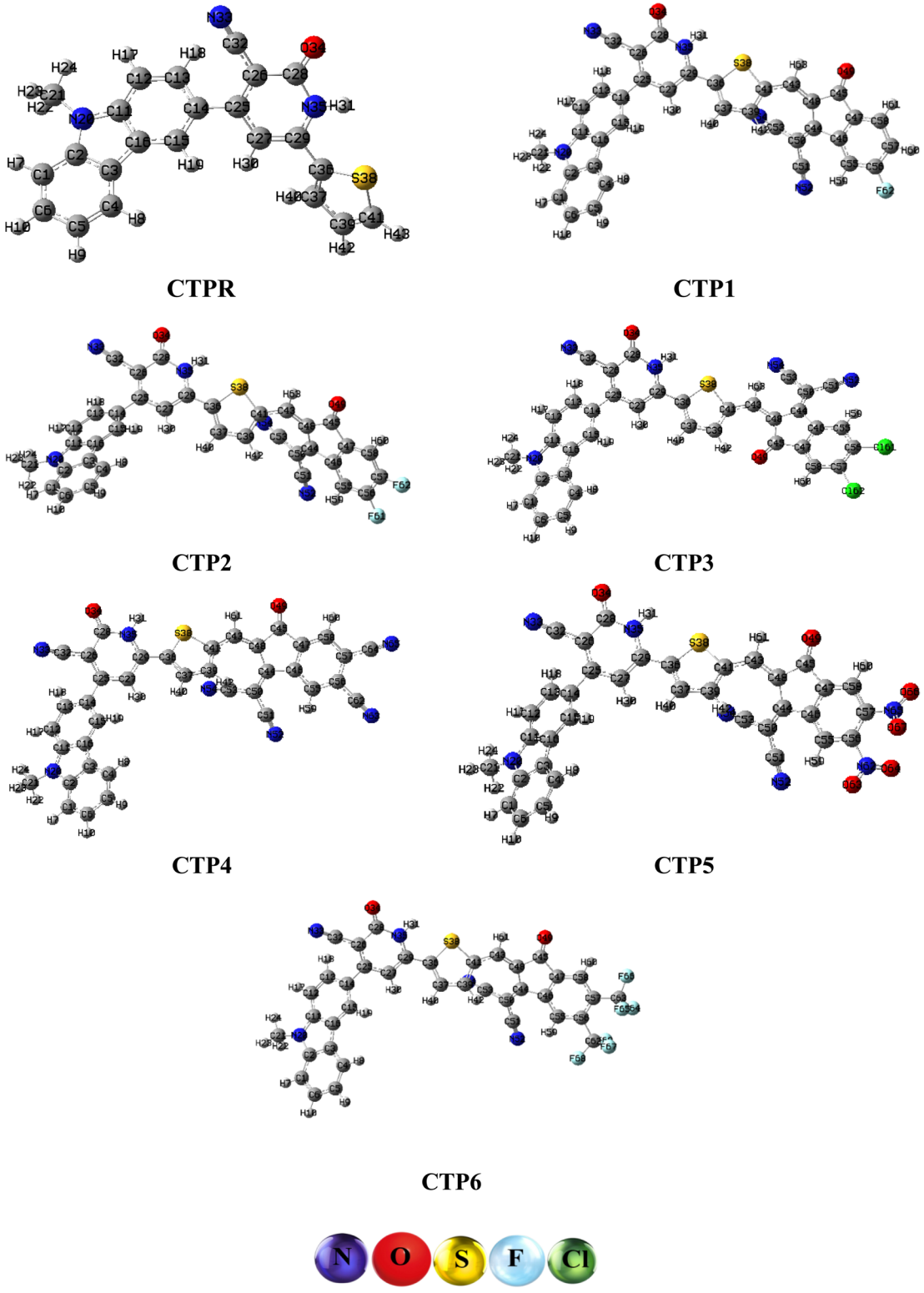

Fig. 2 Optimized geometries of designed compounds (**CTPR–CTP6**) obtained at the M06/6-311G(d,p) level of theory.

might be due to the strong π-electron delocalization between donor, π-spacer and acceptor, and the absence of steric hindrance. This planarity enhances orbital overlap and promotes efficient charge transfer.

The reference compound **CTPR** displays a slightly higher MPP value (0.720 Å), which suggests a moderately planar geometry. The slight deviation is due to torsional strain between the donor and the π-linker, which makes the conjugated backbone twist slightly. However, the molecule continues to

© 2026 The Author(s). Published by the Royal Society of Chemistry

Open Access Article. Published on 08 May 2026. Downloaded on 5/10/2026 4:06:46 PM. This article is licensed under a Creative Commons Attribution-NonCommercial 3.0 Unported Licence.

Table 1 Planarity parameters for the investigated compounds

Compounds	MPP (Å)	SDP (Å)	MPD (Å)	MND (Å)
CTPR	0.720	2.740	1.334	−1.407
CTP1	0.525	2.508	1.265	−1.243
CTP2	0.531	2.539	1.262	−1.278
CTP3	0.780	3.563	1.911	−1.651
CTP4	0.830	3.770	1.972	−1.798
CTP5	0.810	3.767	2.182	−1.585
CTP6	0.866	3.782	2.191	−1.590

have a reasonable coplanarity and electronic contact between its subunits. Conversely, compounds **CTP3–CTP6** have increased MPP values (0.780–0.866 Å), which implies reduced planarity. This may be due to steric congestion and electrical repulsion generated by more electron-drawing substituents on the acceptor end. In conclusion, smaller, planar molecules with strongly electron-drawing substituents but less sterically hindered structures (**CTP1**, **CTP2**) retain their high planarity and efficient π-delocalization, which favors charge transfer and optical activity. Bulky or highly polarizable groups (**CTP3–CTP6**), in their turn, experience higher torsion and reduced coplanarity, which leads to low conjugation. The overall planarity trend is as follows: **CTP1** < **CTP2** < **CTPR** < **CTP3** < **CTP5** < **CTP4** < **CTP6**. Both the steric and electronic effects of the substituents have a significant influence on the planarity of the molecules, the charge transport, and the optical functionality of the D–π–A systems.

Frontier molecular orbitals (FMOs)

The FMO analysis is a significant method for assessing the optoelectronic properties of a molecule.[35–37] The HOMO and LUMO denote the molecule's tendency to donate and accept an electron, respectively, with a smaller energy gap between them indicating stronger CT interactions.[38–41] Molecules with a small energy gap are generally classified as soft, indicating higher reactivity and lower stability.[42] Conversely, electronic systems with a large energy gap are hard, signifying lower reactivity and greater stability (Fig. 3).[43,44]

The Kohn–Sham HOMO–LUMO energy gap of the reference molecule **CTPR** is large, at 3.802 eV. Although this large gap can qualitatively indicate a weaker ICT character, it is important to remember that the Kohn–Sham gap itself is a functional-dependent artifact of DFT and, unlike excitation energies, is not an observable quantity. There are structural adjustments that result in observable decreases in this KS gap of the designed derivatives. The qualitative interpretation of this trend is an increase in electronic interaction and coupling between the donor and acceptor portions of the molecule, which is a requirement for strong NLO activity.

A moderate reduction in the KS ΔE of the chromophores **CTP1** and **CTP2** (to 2.668 and 2.677 eV, respectively) is in line with the electron-withdrawing character of the fluoro and difluoro substituents that stabilize the LUMO. On the same note, **CTP3** exhibits a small reduction in the KS gap (2.604 eV) upon replacement with the dichloro group. The largest decreases in the KS gap are found in **CTP4** (2.385 eV) and **CTP5** (2.327 eV). Although these small KS gaps are a sign of high donor–acceptor couplings, the real NLO potential of these gaps is not the gap value, but the character of the low-lying electronic transitions, which should be determined by methods such as TD-DFT. Pictograms and values of HOMO−1, LUMO+1, HOMO−2, LUMO+2, and their energy gaps in eV are presented in Fig. S2 and Table S9.

The enhanced NLO potentials of **CTP4** and **CTP5** are explained with the help of the electronic density distribution of the frontier molecular orbitals (FMOs). The HOMO and LUMO in **CTPR** are relatively localized, indicating that there is limited electron-density migration during excitation. Conversely, **CTP4** and **CTP5** have a distinct separation in space: in the HOMO, the electronic cloud is mostly concentrated on the donating moiety, whereas in the LUMO, it is dispersed by the area of the electron acceptor with the dicyano or dinitro functional groups. Such a strong HOMO–LUMO decoupling is a characteristic of effective ICT and the main source of their improved first- and third-order hyperpolarizabilities. The strong donor–acceptor separation leads to reduced HOMO–LUMO spatial overlap, which enhances charge-transfer character and contributes to a smaller Kohn–Sham energy gap. The uniform reduction in LUMO energy of all derivatives relative to **CTPR** provides further evidence of their better electron-accepting capability, which facilitates the process of charge transfer that is necessary for NLO responses. To conclude, the Kohn–Sham HOMO–LUMO gap is an effective qualitative indicator of trends in a congeneric series, although the ultimate evaluation of NLO performance must be made by a detailed examination of excited-state properties, transition dipole moments, and hyperpolarizabilities obtained using more complex theories.

The stability and chemical reactivity obtained using the HOMO–LUMO energies of the designed compounds are explained using global reactivity parameters. These parameters include ionization potential (IP),[45] electron affinity (EA),[46] chemical potential (μ),[47] global hardness (η),[48] electronegativity (X),[49] global electrophilicity (ω), and global softness (σ).[50,51] The global hardness (η) of the reference molecule **CTPR** reflects its resistance to charge transfer, indicating its low reactivity. Conversely, the designed derivatives have significantly lower η values, indicating greater charge-transfer ability and polarization under external electric fields, especially **CTP5** and **CTP4**. While global softness (σ), the reciprocal of hardness, increases across the derivatives, suggesting higher polarizability. Detailed values of the global reactivity descriptors are presented in Table S10, while detailed equations are displayed in the SI S1–S8.

UV-Visible absorption analysis

TD-DFT computations were conducted in both liquid and gaseous phases to evaluate the UV-Visible absorption spectra of the studied compounds. Table 2 displays significant variables, such as oscillator strength (f_{os}), excitation energy (E), excitation wavelength (λ), and the variety of molecular orbital (MO) transitions. These features play a crucial role in determining the photophysical behavior and NLO performance of the

Open Access Article. Published on 08 May 2026. Downloaded on 5/10/2026 4:06:46 PM.
This article is licensed under a Creative Commons Attribution-NonCommercial 3.0 Unported Licence.

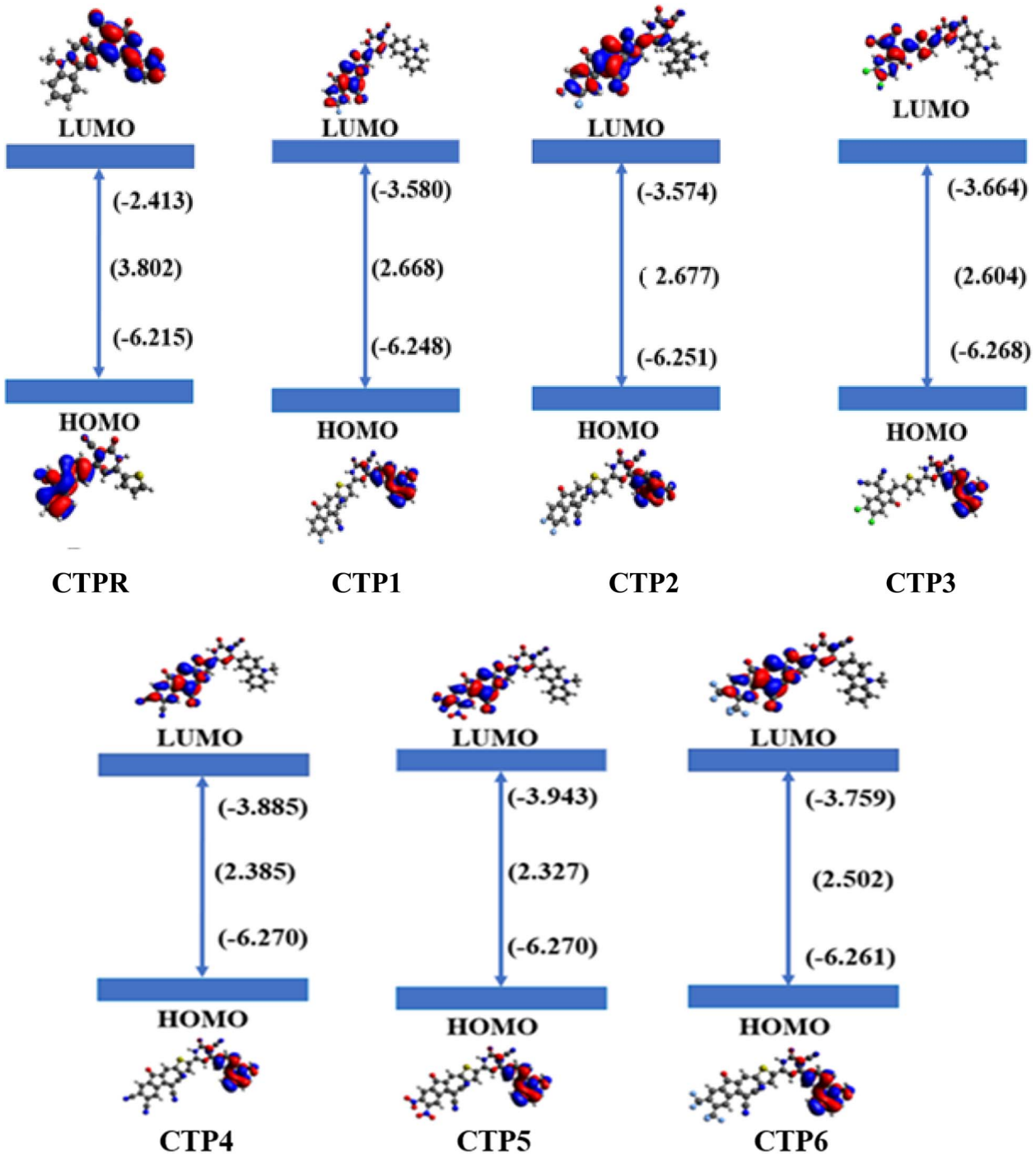

Fig. 3 Calculated HOMO and LUMO energy levels along with their corresponding molecular orbital isosurfaces for all the studied compounds at the M06/6-311G(d,p) level of theory.

compounds.[52] The six lowest transitions are listed in Tables S11–S24.

Table 2 indicates that, in the solvent phase, **CTPR** has the highest absorption at 368.07 nm with an excitation energy of 3.369 eV and a moderate oscillator strength ($f_{os} = 0.538$), which is a HOMO−2 to LUMO (52%) transition. When the structure is altered, a unique bathochromic shift in the absorption peaks of the derivatives is observed, indicating increased π-conjugation and efficient ICT. It is interesting to note that **CTP4** and **CTP5** have pronounced redshifts, with absorption maxima at 553.85 nm and 559.57 nm, respectively, which signify low excitation energies of 2.239 eV and 2.216 eV, respectively. These redshifts coincide with the lower HOMO–LUMO energy gaps that were found in the FMO study. On the same note, the chromophore **CTP3** was found to exhibit intense absorption with strong oscillator strengths ($f_{os} = 1.269$ and 1.129, respectively), implying transition probabilities. The absorption spectra in the gaseous phase follow the same pattern, with

© 2026 The Author(s). Published by the Royal Society of Chemistry

Open Access Article. Published on 08 May 2026. Downloaded on 5/10/2026 4:06:46 PM. This article is licensed under a Creative Commons Attribution-NonCommercial 3.0 Unported Licence.

Table 2 Computed UV-Vis values of CTPR and CTP1–CTP6 in chloroform and the gaseous phase[a]

Phases	Compounds	DFT λ (nm)	E (eV)	f_{os}	MO contributions
Solvent phase	**CTPR**	368.07	3.369	0.538	H−2 → L (52%)
	CTP1	516.41	2.401	0.728	H−2 → L (88%)
	CTP2	512.14	2.421	0.668	H−2 → L (90%)
	CTP3	508.210	2.439	1.269	H−2 → L (93%)
	CTP4	553.85	2.239	0.699	H−2 → L (93%)
	CTP5	559.57	2.216	0.594	H−2 → L (91%)
	CTP6	534.18	2.321	0.728	H−2 → L (93%)
Gaseous phase	**CTPR**	367.14	3.377	0.430	H−1 → L (89%)
	CTP1	535.52	2.315	0.504	H−2 → L (65%)
	CTP2	537.38	2.307	0.526	H−2 → L (71%)
	CTP3	510.03	2.431	0.483	H−2 → L (72%)
	CTP4	578.74	2.142	0.463	H−2 → L (95%)
	CTP5	584.25	2.122	0.406	H−2 → L (92%)
	CTP6	552.76	2.243	0.387	H−2 → L (84%)

[a] MO = molecular orbital, H = HOMO, L = LUMO, f_{os} = oscillator strength, and λ (nm) = wavelength.

a slight variation in the spectra. The parent compound **CTPR** has an absorption at 367.14 nm with an excitation energy of (3.377 eV), which has a low oscillator strength. However, the designed derivatives, particularly **CTP4** and **CTP5**, exhibit strong redshifted absorptions at 578.74 nm and 584.25 nm, which are associated with lower excitation energies of 2.142 eV and 2.122 eV, respectively. These outcomes confirm that there is an increase in ICT and molecular polarizability in both phases upon altering the end-capped acceptor groups.

Gaussian-broadened MO spectrum

Analysis of the Gaussian-broadened MO spectrum reflects the number of electronic conditions that can be seen at specific energy levels and gives significant information on the energetic changes and the general electronic structure.[53] To further explore the electronic properties of **CTPR** and **CTP1–CTP6** and corroborate the FMO results, Gaussian-broadened MO spectral analysis was performed, as shown in Fig. 4. The Gaussian-broadened MO plots are used to show the distribution of electrons between the HOMO and LUMO regions, with the *x*-axis representing the energy and the *y*-axis being the relative intensity. The results of the quantitative contribution of the donor, π-spacer, and acceptor fragments to the FMOs of the compounds studied are summarized in Table S25. The electronic cloud in HOMOs are predominantly localized on the donor units (94.2–94.6%), with minor π-spacer involvement (5.4–5.7%) and negligible acceptor contribution, highlighting ground-state electron density and efficient ICT. In contrast, in LUMOs, the electron density displays greater variability as they are mainly localized on the π-spacer (91.3%) for **CTPR**, whereas in the designed derivatives **CTP1–CTP6**, a distinct shift toward the acceptor regions is observed, particularly for **CTP5** (83.4%) and **CTP4** (78.1%), indicating enhanced electron-withdrawing behavior and improved ICT efficiency. Detailed orbital contribution trends are provided in Table S25. Acceptor involvement in the HOMOs is negligible in all compounds, except **CTP2** and **CTP6**, which both have a marginal 0.1% contribution. The HOMO mostly resides in the donor segment, and the LUMO is primarily located in the acceptor segment, with the π-spacer facilitating charge transfer.

The orbital composition pictographs (Fig. 4) depict the electron distributions in terms of donor (red), π-spacer (green) and acceptor parts (blue), with the total orbital composition shown in black. The remarkably good agreement between orbital localization and orbital composition analysis qualitatively indicates that smaller HOMO–LUMO gaps can be associated with ICT and better charge delocalization. This electronic behavior suggests an enhancement in molecular polarizability and further substantiates the anticipated qualitative trends in the second- and third-order NLO responses of these compounds.

Transition density matrix (TDM)

The transition density matrix (TDM) serves as an effective tool to explore the transition processes and the rate of ICT in a conjugated system. The three-dimensional TDM plots offer visual images of donor–acceptor interactions in the excited-state species and reveal the electron–hole localization. Hydrogen atoms make little contribution to electronic transitions therefore, excluded from this analysis.

The **CTPR** heat map showed a high intensity mainly about the D–π region, evidencing strong excitation localization at the D–π interface. This behavior indicates the presence of limited charge transfer, where electron density mainly transfers from the donor orbitals to the π-conjugated part, showing weak ICT. On the other hand, the TDM of **CTP1**, shown in Fig. 5, demonstrated a broader and less localized charge-transfer pathway. In comparison to **CTPR**, the motion of electron density spread was more extended along the π-bridge to the acceptor segment, which indicated a higher conjugation and interaction among molecules. The **CTP1** drives the increase in charge separation and indicates a possible increase in charge mobility, resulting in improved optoelectronic properties. In contrast, compound **CTP2** had a much more dispersed transition density along the D–π–A axis. The TDM complex plot indicates defined contact sites with the donor/acceptor through the π-system, indicating better charge transport in the

Open Access Article. Published on 08 May 2026. Downloaded on 5/10/2026 4:06:46 PM.
This article is licensed under a Creative Commons Attribution-NonCommercial 3.0 Unported Licence.

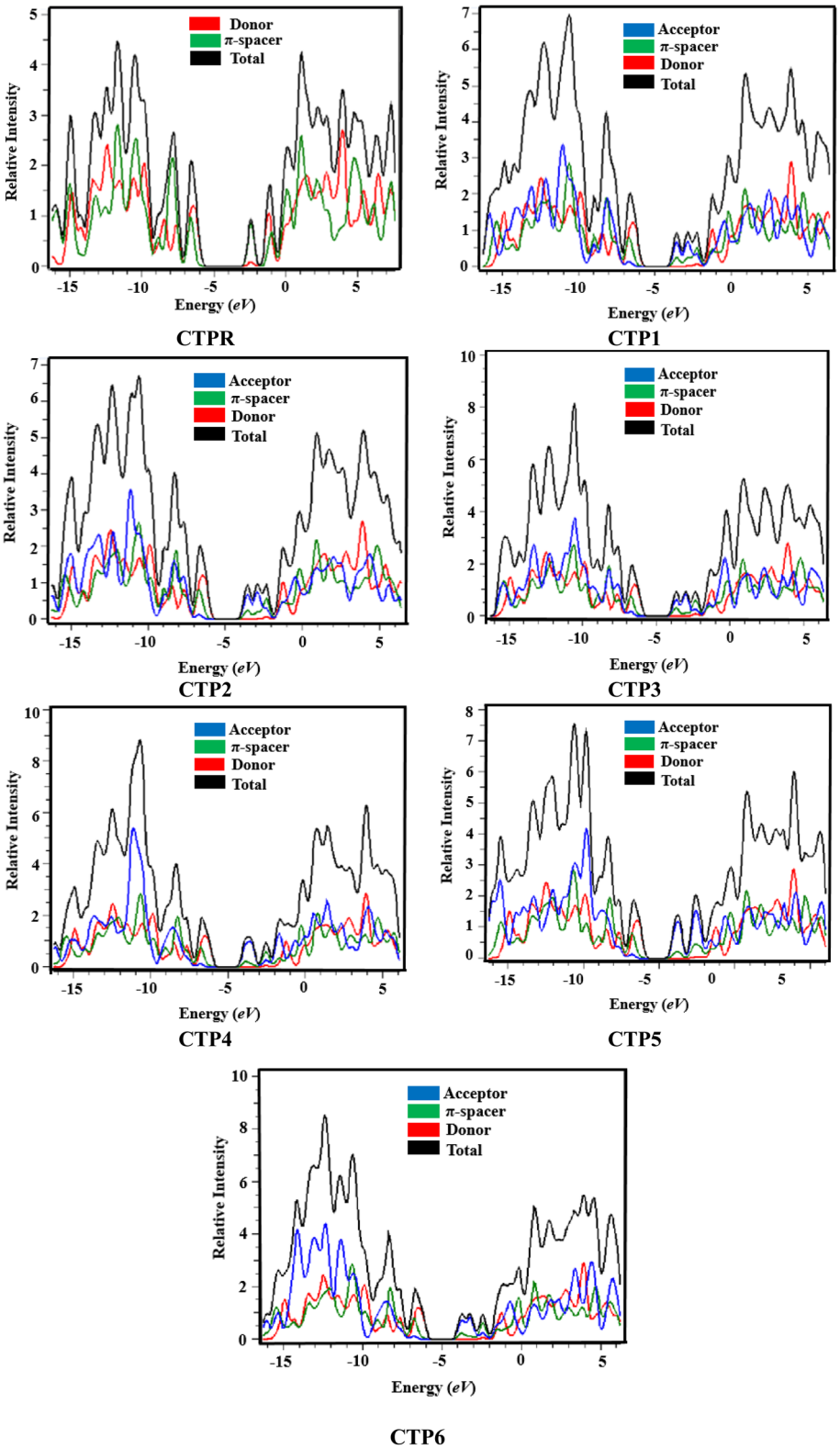

Fig. 4 Gaussian-broadened MO plots of the designed compounds CTPR–CTP6, illustrating the electronic cloud probability at different parts of the chromophores.

molecule. This means that **CTP2** has better alignment of its FMOs, which leads to charge transfer over longer distances and an increase in the NLO response.

The charge transfer in **CTP4** and **CTP5** through the π-spacer between the acceptor and donor is efficient. The above results from TDM analysis indeed show the migration of excitations in

© 2026 The Author(s). Published by the Royal Society of Chemistry

Open Access Article. Published on 08 May 2026. Downloaded on 5/10/2026 4:06:46 PM.
This article is licensed under a Creative Commons Attribution-NonCommercial 3.0 Unported Licence.

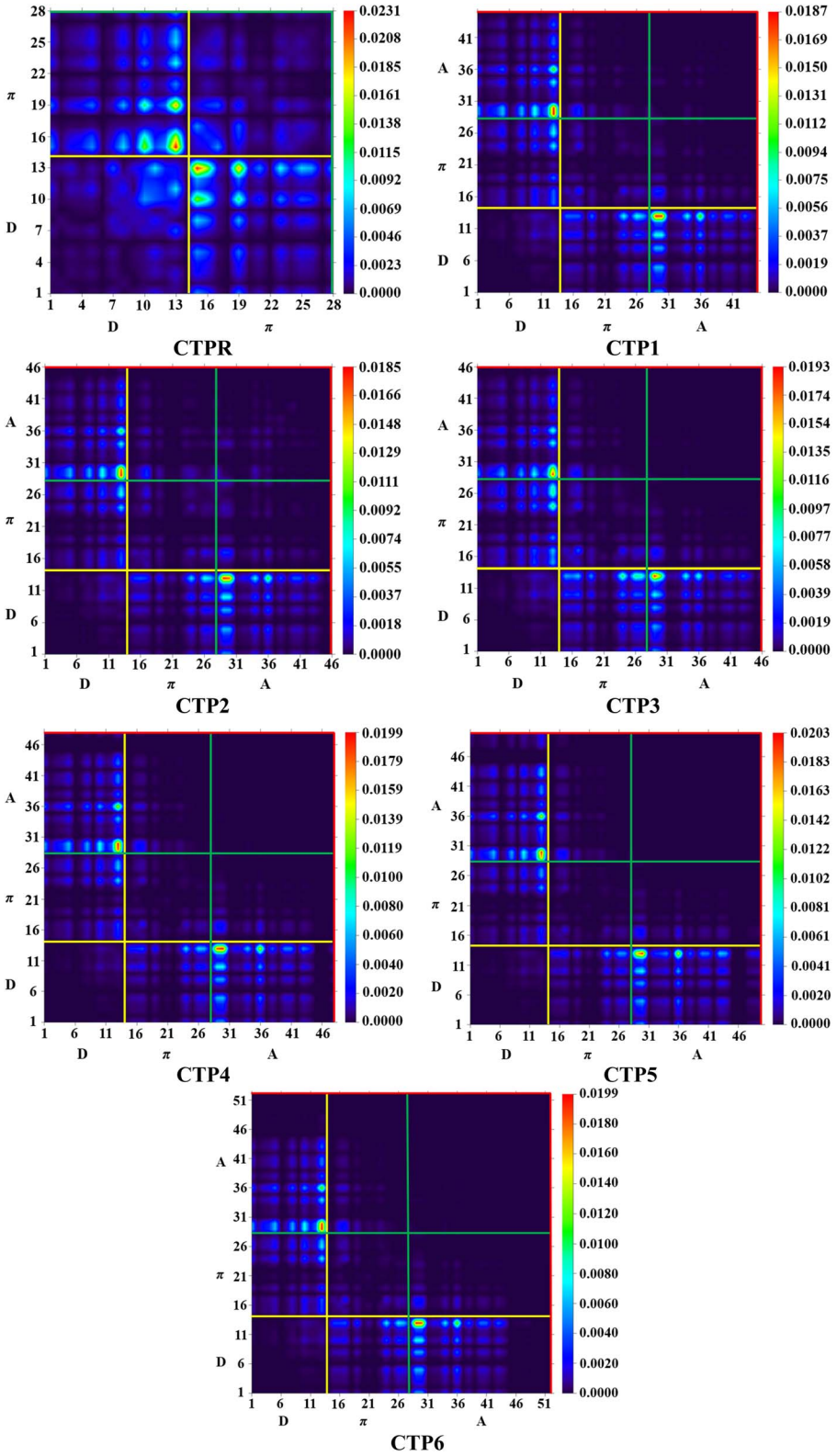

Fig. 5 TDM heat maps for **CTPR–CTP6**, illustrating S_0 to S_1 transitions.

CTPR and **CTP1–CTP6**. This means that the donor and π-spacer units can be modified to greatly affect the CT process, which is effective for improving the NLO and optoelectronic properties of these compounds.

Hole–electron analysis

The electron–hole analysis provides useful information with respect to the charge carriers and excitations present in the designed materials **CTP1–CTP7**.[54] Based on the analysis

Open Access Article. Published on 08 May 2026. Downloaded on 5/10/2026 4:06:46 PM.
This article is licensed under a Creative Commons Attribution-NonCommercial 3.0 Unported Licence.

performed with Multiwfn 3.8, it is found that all the designed compounds have substantial ICT. The hole state distribution is mainly kept on the sulfur atom of the thiophene π-spacer, and the electron density is on the acceptor position (in particular on C25), supporting efficient charge transfer from the donor to the acceptor part. The sulfur-based π-spacer plays a dominant role in charge redistribution, leading to asymmetric charge separation, which might lead to an enhanced NLO response through an increase in the molecular hyperpolarizability. As shown in Fig. 6, several holes are localized on the π-linker between the donor and acceptor; electron density is largely centered on the acceptor portions. The hole–electron analysis of the excitation of S_0 to S_1 makes a valuable contribution to the study of the charge-transfer properties of the entitled chromophores (Table S37). It is observed that the excitation energies decrease from **CTPR** (3.115 eV) to **CTP5** (1.956 eV), which supports the evidence that the structural modification is successful in reducing the optical energy gap and promoting the movement of electrons within the designed derivatives. In all the compounds, the centroid distance between the hole and electron of the compound is highest in **CTPR** (D index = 2.310 A), and the overlap integral is the largest ($S_r = 0.35395$), indicating a balanced role of local excitation and charge transfer.

Conversely, the derivatives **CTP1–CTP6** exhibit relatively low S_r values (0.0978–0.2186), suggesting a stronger charge-transfer nature and less overlap between the holes and electrons. The breadth of hole and electron distribution, as characterized by H (Å), is marginally larger in derivatives with the largest value of (3.613 Å), which corresponds to **CTP2**, meaning that charge density is more spatially segregated. The HDI and EDI values also confirm this point, with the derived indices (HDI ≈ 8.0–8.5 and EDI ≈ 5.8–6.2) indicating stabilized electron–hole distributions on the molecular framework.

It is worth noting that both the excitation energy of **CTP4** and **CTP5** and their S_r values are lower, meaning that the ICT is more pronounced, which is favorable for the NLO response. The hole–electron analysis in general indicates that structural tuning of the designed chromophores is a good method for improving the charge separation as well as the ICT properties over those of the reference compound, and can enhance their optoelectronic and NLO activity.

Molecular electrostatic potential

The molecular electrostatic potential (MEP), shown in Fig. 7, exhibits regions of nucleophilicity (red) along with electronegative regions on the dihydropyridine. The nature of the MEP is determined by the distribution of electron density; high electron density occurs in the regions marked in red, which means that these sites possess a negative electrical potential (nucleophilic). Low electron density is indicated by blue areas with positive electrical potential (electrophilic).[55] On the MEP map, O atoms positioned in the red regions function as nucleophiles, whereas H atoms in the blue regions are electrophiles. These reactive regions are essential for identifying potential interaction sites and predicting favorable binding conformations of the molecule.

Natural bond orbitals (NBO)

Natural bond orbital (NBO) analysis offers valuable insights into the nature of chemical bonding and electronic interactions

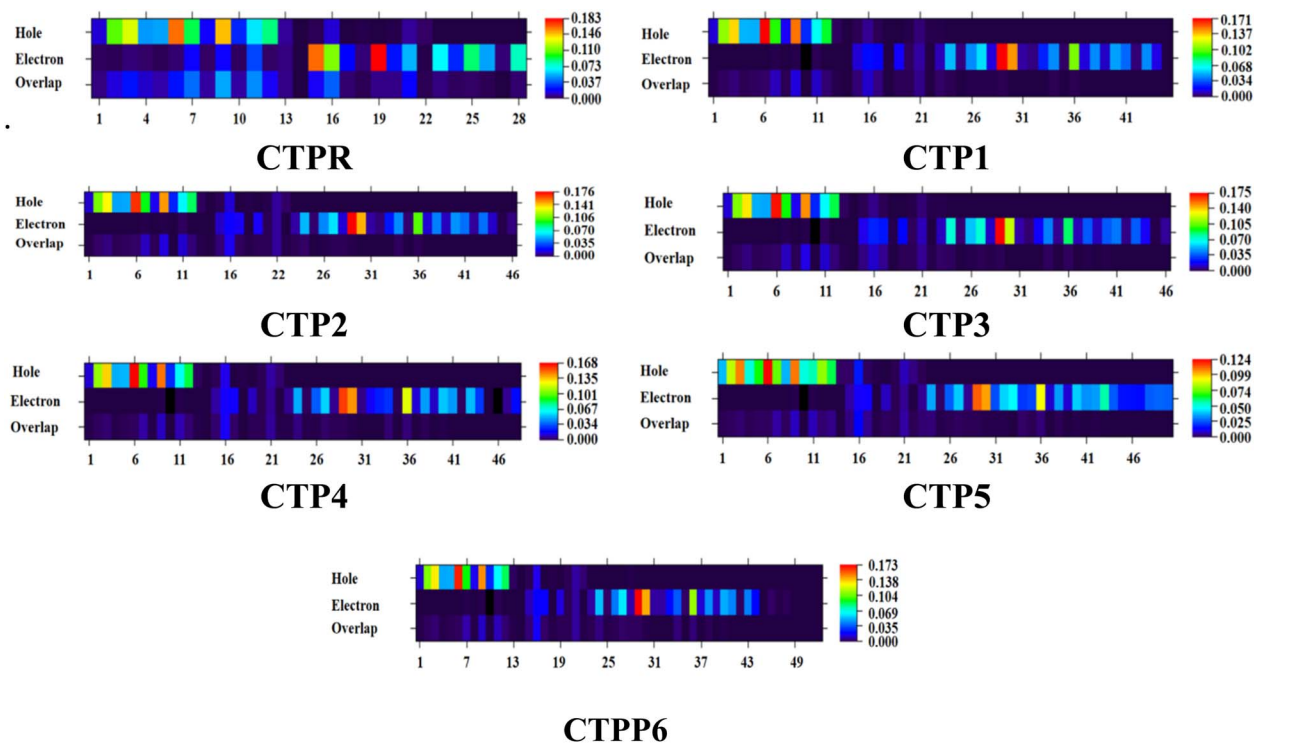

Fig. 6 Pictorial representation of hole–electron transport analysis.

© 2026 The Author(s). Published by the Royal Society of Chemistry

Open Access Article. Published on 08 May 2026. Downloaded on 5/10/2026 4:06:46 PM.
This article is licensed under a Creative Commons Attribution-NonCommercial 3.0 Unported Licence.

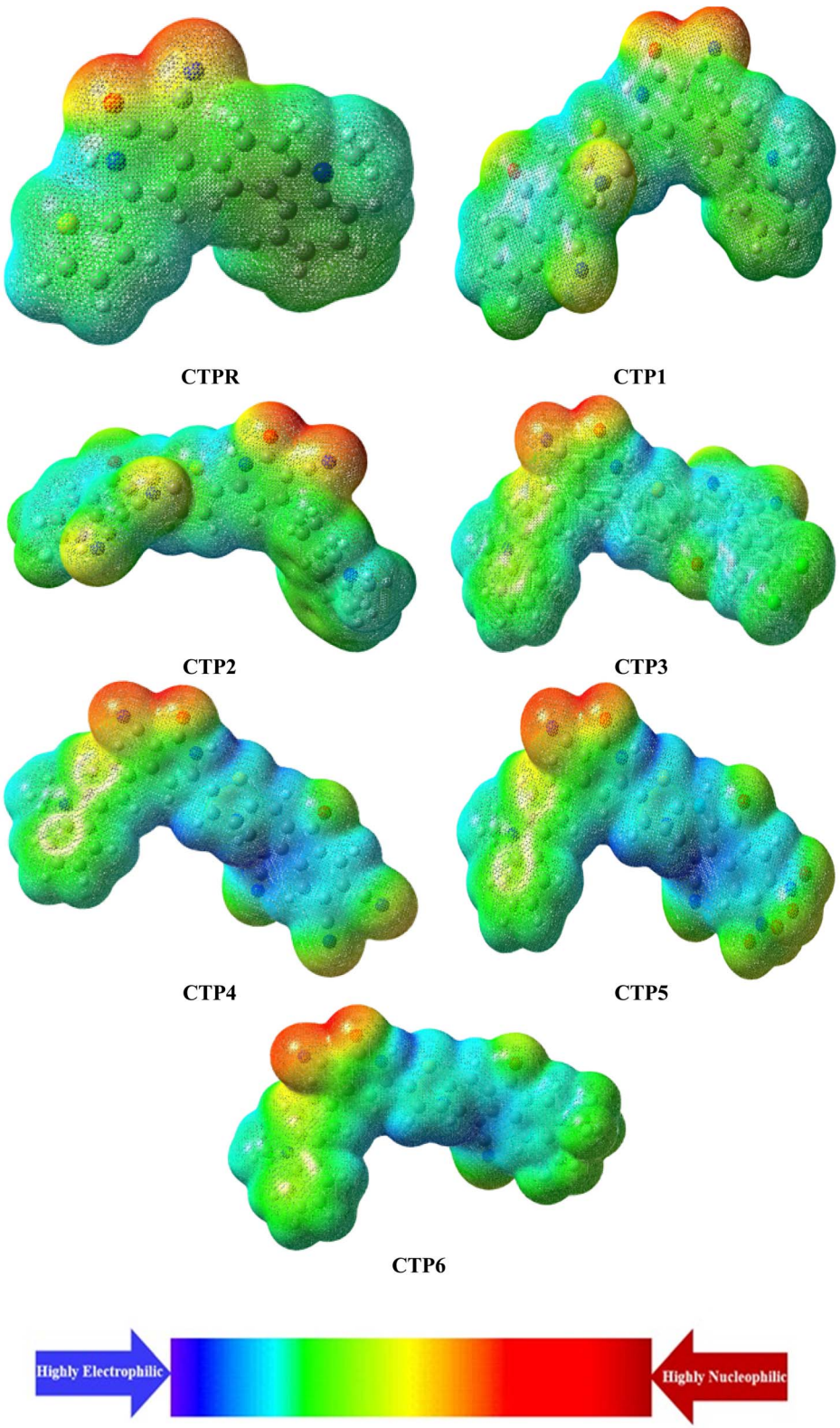

Fig. 7 MEP pictographs of CTPR–CTP6, showing the nucleophilic and electrophilic regions of the entitled compounds.

within molecules. It explains various intramolecular and intermolecular charge-transfer interactions and provides information on the nature of charge distribution in organic systems. NBO analysis is used extensively to determine natural charges in donor–π–acceptor (D–π–A) frameworks. In the present study, NBO analysis was performed on the investigated compounds to

Open Access Article. Published on 08 May 2026. Downloaded on 5/10/2026 4:06:46 PM. This article is licensed under a Creative Commons Attribution-NonCommercial 3.0 Unported Licence.

evaluate the second-order perturbation stabilization energy $E^{(2)}$, which serves as a key indicator of charge delocalization and hyperconjugative interactions.[56] The stabilization energy (*i.e.*, $E^{(2)}$) for each donor (i) to acceptor (j) transition, indicating $i \rightarrow j$ delocalization, is calculated using eqn (9).

$$E^{(2)} = q_i \frac{(F_{i,j})^2}{\varepsilon_j - \varepsilon_i} \quad (9)$$

Here, $E^{(2)}$ represents the stabilization energy, E_i and E_j are the orbital energies of the donor and acceptor, respectively, q_i is the occupancy of the donor orbital, and $F_{(i,j)}$ is the Fock matrix element between the NBOs.[57] The summarized results are presented in Table S33, while detailed values are provided in Tables S26–S32.

The parent compound, **CTPR**, exhibits significant $\pi \rightarrow \pi^*$ and lone pair (LP) $\rightarrow \pi^*$ delocalization with higher stabilization energies. The π(C16–C18) $\rightarrow \pi^*$(C13–C15) interaction exhibits a stabilization of 23.56 kcal mol^{-1}, whereas the LP(N1) $\rightarrow \pi^*$(C2–C4) interaction demonstrates a stabilization of 24.86 kcal mol^{-1}. This indicates that nitrogen rapidly donates its charge to the conjugated backbone. For the derivatives, **CTP1** exhibits a stronger ICT than **CTPR**. Among all the derivatives, **CTP1–CTP4** displayed significant $\pi \rightarrow \pi^*$ interactions and LP(N1) $\rightarrow \pi^*$(C2–C4) transitions, contributing 25–37 kcal mol^{-1}, with strong donor–acceptor overlap. This indicates the role of the heteroatoms in enhancing ICT. The highest charge-transfer network is found in **CTP5**, where the interaction between π and LP is synergistic; *i.e.*, an LP(N1) $\rightarrow \pi$ (C2–C4) at 28.23 kcal mol^{-1}. **CTP6** exhibits similar stabilization energies (25–36 kcal mol^{-1}), with the electron delocalization in the conjugated framework being supported by $\pi \rightarrow \pi^*$ and LP $\rightarrow \pi^*$interactions.

In summary, it expolites that structural changes enhance intramolecular charge transfer, particularly when the appropriate positions of nitrogen and sulphur atoms are included. These findings underscore the structure–property relationships, highlighting the role of structural modifications in tuning NLO properties.

Non-linear optical properties

Polarizability and hyperpolarizability are important for understanding the structure–property correlation of molecules for potential NLO properties. High values of polarizability, large dipole moments, and high hyperpolarizabilities lead to good NLO performance. Linear polarizability ($\langle\alpha\rangle$) describes the extent to which an applied electric field can distort a molecule's electron cloud, while hyperpolarizability (β, γ) reflects the intrinsic atomic and molecular contributions to various nonlinear optical effects.[58] The computed β_{total} values and major contributing tensor of derived compounds are given in Table 3.

The dipole moment values vary significantly among the examined compounds, ranging from the lowest at 6.6900 D (**CTP5**) to 12.6704 D (**CTPR**). The highest dipole moment, observed for **CTPR**, reflects its enhanced ICT character, suggesting stronger donor–acceptor interactions. Among the designed derivatives, **CTP1** (9.2204 D) and **CTP2** (10.0615 D) maintain relatively high polarity, supporting efficient donor–acceptor interactions. *para*-Nitroaniline (*p*-NA) is used as a reference compound and, according to the literature, its standard dipole moment is 4.9662 D. It is observed here that all the derivatives have higher dipole moments than *p*-NA.[59] The dipole moment follows the ascending order: **CTPR** (12.67) < **CTP2** (10.06) < **CTP3** (8.74) < **CTP6** (6.90) < **CTP4** (6.84) < **CTP5** (6.70).

The average polarizability ($\langle\alpha\rangle$) values show a gradual increase from 0.6992×10^{-23} esu (**CTPR**) to 1.321×10^{-22} esu (**CTP1**). All designed derivatives exhibit higher $\langle\alpha\rangle$ values than the reference compound **CTPR**, indicating enhanced electronic delocalization facilitated by donor–π–acceptor interactions and incorporation of diverse acceptor units. The $\langle\alpha\rangle$ values are in the following descending order: **CTP1** (1.321×10^{-22} esu) > **CTP4** (1.443×10^{-22} esu) ≈ **CTP5** (1.421×10^{-22} esu) > **CTP6** (1.381×10^{-22} esu) > **CTP3** (1.356×10^{-22} esu) > **CTP2** (1.260×10^{-22} esu) > **CTPR** (6.992×10^{-23} esu). Table S34 shows the dipole polarizability and dominant tensor component (in esu) of the studied chromophores using different diffuse basis sets.

The first hyperpolarizability (β_{total}) serves as a key parameter for evaluating the NLO response. Among all the studied compounds, **CTP4** exhibits the highest β_{total} (9.279×10^{-28} esu), significantly surpassing that of the reference **CTPR**, reflecting its superior NLO efficiency. Similarly, **CTP5** (9.012×10^{-28} esu) also demonstrates remarkable enhancement compared to the reference. All derivatives have higher β_{total} values than *p*-NA, which is 3.610×10^{-31} esu.[59] The descending trend is: **CTP4** (9.279×10^{-28} esu) > **CTP5** (9.012×10^{-28} esu) > **CTPR** (8.172×10^{-29} esu) > **CTP6** (7.977×10^{-28} esu) > **CTP3** (6.478×10^{-28} esu) > **CTP1** (6.287×10^{-28} esu) > **CTP2** (5.836×10^{-28} esu). Notably, **CTP4** and **CTP5** exhibit the highest β values, which can be attributed to stronger push–pull electronic effects and extended π-conjugation, facilitating efficient charge transfer across the molecular backbone. Table S35 shows the computed first hyperpolarizability (β_{total}) and major contributing tensors (esu).

The second hyperpolarizability (γ_{total}) exhibited a consistent pattern under these conditions, which varies between 4.993×10^{-34} esu (**CTPR**) and 6.144×10^{-33} esu (**CTP4**), with the order: **CTP4** > **CTP5** > **CTP6** > **CTP2** > **CTP3** > **CTP1** > **CTPR**. Similarly,

Table 3 Dipole moment, polarizability, and hyperpolarizabilities of the investigated compounds (CTPR and CTP1–CTP6) using diffuse basis sets[a]

Compounds	μ^{D}_{total}	$\langle\alpha\rangle \times 10^{-22}$	$\beta_{total} \times 10^{-28}$	$\gamma_{total} \times 10^{-33}$
CTPR	12.6704	0.0699	0.817	0.499
CTP1	9.2204	1.321	6.287	4.641
CTP2	10.0615	1.260	5.836	4.623
CTP3	8.7466	1.356	6.478	4.942
CTP4	6.8493	1.434	9.279	6.144
CTP5	6.6990	1.421	9.012	5.991
CTP6	6.8985	1.381	7.977	5.229

[a] μ^{D}_{total} in D; $\langle\alpha\rangle$, β_{total} and γ_{total} in esu.

© 2026 The Author(s). Published by the Royal Society of Chemistry

Open Access Article. Published on 08 May 2026. Downloaded on 5/10/2026 4:06:46 PM. This article is licensed under a Creative Commons Attribution-NonCommercial 3.0 Unported Licence.

the magnitude of γ follows: **CTP4** (4.231×10^{-33} esu) > **CTP5** (4.130×10^{-33} esu) > **CTP6** (3.611×10^{-33} esu) > **CTP3** (3.543×10^{-33} esu) > **CTP2** (3.209×10^{-33} esu) > **CTP1** (3.202×10^{-33} esu) > **CTPR** (3.914×10^{-34} esu), confirming that substitution significantly enhances the third-order NLO properties.

Among all the derivatives, **CTP4** emerges as the most promising candidate for NLO applications, owing to its exceptionally high dipole moment, polarizability, and both first- and second-order hyperpolarizabilities. The frequency-dependent NLO responses of the designed compounds were calculated at laser wavelengths of 532 nm ($\omega = 0.042823$ esu) and 1064 nm ($\omega = 0.085645$ esu), as summarized in Table S36. These properties encompass the electro-optic pockels effect (EOPE), $\beta(-\omega, \omega, 0)$, and second-harmonic generation (SHG), $\beta(-2\omega, \omega, \omega)$, corresponding to the first-order responses, as well as the electro-optic Kerr effect (EOKO), $\gamma(-\omega, \omega, 0, 0)$, representing the third-order nonlinear response. These evaluations were performed to assess the potential of the studied systems for frequency-dependent NLO applications. From Table S36, it is evident that the first hyperpolarizability values exhibit strong wavelength dependence. At 532 nm, the $\beta(-\omega, \omega, 0)$ and $\beta(-2\omega, \omega, \omega)$ values are markedly higher for most derivatives compared to the static field. When compared to TD-DFT excitation energies, the S1 transition is found to be around 2.21–2.45 eV in the considered systems, so the frequency of 532 nm is in the vicinity of the electronic resonance. This near-resonant condition leads to significant enhancement of β values relative to the static limit. Conversely, 1064 nm is farther from the main excitation energy, so it shows only moderate enhancement. Thus, the high frequency-dependent β values are caused by resonance effects and not necessarily intrinsic electronic nonlinearity. Notably, **CTP4** demonstrates an exceptionally large $\beta(-\omega, \omega, 0)$ of 1.704×10^{-21} esu and $\beta(-2\omega, \omega, \omega)$ of 5.057×10^{-29} esu, indicating its strong response toward external electric fields and significant potential for first-order NLO processes. Among the other derivatives, **CTP5** and **CTP6** also display relatively high β values, suggesting pronounced charge-transfer characteristics under the applied frequencies. The third-order NLO responses (Table S36) further reinforce the wavelength-dependent behavior.

A standard reference NLO molecule is *para*-nitroaniline (*p*-NA), and the first hyperpolarizability of this molecule is normally approximately 6.3×10^{-30} esu. By comparison, the β_{total} values of all the examined chromophores are significantly larger, in the range of 10^{-28} esu, which is roughly 100–1000 times higher than that of *p*-NA. This significant improvement underscores the high NLO activity of the developed systems, especially **CTP4** and **CTP5**, owing to their good donor–π–acceptor structure and improved charge-transfer properties. Thus, these chromophores offer good prospects for high-tech optoelectronic and photonic applications. All of these results suggest that the NLO responses are closely dependent on the probed frequency; **CTP4** and **CTP5** exhibit enhanced performance in electro-optic and harmonic generation. These findings demonstrate the tunability of the designed chromophores for specific optoelectronic, photonic and telecommunication applications.

Conclusion

Here, the **CTPR** derivatives were designed for use in NLO materials by structural modeling with efficient acceptors at one terminal. The electron withdrawing groups were introduced at the terminal acceptors to improve the push–pull framework which improved ICT and efficiency for NLO property in entitled compounds. The designed electron-acceptor D–π–A chromophores exhibited tunable electronic and optical properties with energy gaps in the range of 2.327 to 3.802 eV and subsequent redshifted lowest energy absorption peaks, indicating efficient charge delocalization. Among the studied compounds, **CTP4** exhibited the lowest energy gap (2.327 eV), highest softness (0.429 eV^{-1}), and lowest hardness, suggesting its superior reactivity. The NLO analysis revealed that **CTP4** possesses the highest hyperpolarizability ($\beta_{total} = 9.279 \times 10^{-28}$ esu, $\gamma_{total} = 6.144 \times 10^{-33}$ esu), confirming its robust second- and third-order NLO response. Overall, the newly designed **CTPR** derivatives, especially **CTP4**, emerge as promising candidates for future nonlinear optical and optoelectronic device applications. These results show a clear structure–property relationship. The CTP4 design is suitable for applications needing optical transparency, while for high-performance NLO devices—where strong nonlinear response is key—CTP4 and CTP5 are the most promising systems. It provides a systematic classification that establishes a logical framework for selecting specific CTP-based molecules according to the target optoelectronic application.

Conflicts of interest

There are no conflicts of interest to declare.

Data availability

All data generated or analyzed during this study are included in this published article and its supplementary information (SI) files. Supplementary information is available. See DOI: https://doi.org/10.1039/d5ra09811d.

Acknowledgements

MI extends gratefully appreciation to the Deanship of Research and Graduate Studies at King Khalid University, Saudi Arabia, through small Research Project under grant number RGP-1/239/46.

References

1 *Materials for Nonlinear Optics: Chemical Perspectives*, ed. S. R. Marder, J. E. Sohn and G. D. Stucky, American Chemical Society, Washington, DC, 1991, DOI: 10.1021/bk-1991-0455.
2 Y. Zhang and Y. Wang, Nonlinear optical properties of metal nanoparticles: a review, *RSC Adv.*, 2017, 7, 45129–45144. https://pubs.rsc.org/en/content/articlehtml/2017/ra/c7ra07551k.
3 Z. S. Shanon and R. Sh, Study of the Nonlinear Optical Properties of Lithium Triborate Crystal by Using Z-Scan,

Open Access Article. Published on 08 May 2026. Downloaded on 5/10/2026 4:06:46 PM. This article is licensed under a Creative Commons Attribution-NonCommercial 3.0 Unported Licence.

Int. J. Sci. Res., 2016, 1683, https://www.researchgate.net/profile/Raad-Alnayli/publication/312500234_Study_of_the_Nonlinear_Optical_Properties_of_Lithium_Triborate_Crystal_by_Using_Z-Scan_Technique/links/588e55cb92851cef1362cb37/Study-of-the-Nonlinear-Optical-Properties-of-Lithium-Triborate-Crystal-by-Using-Z-Scan-Technique.pdf.

4 T. H. Maiman, Stimulated optical radiation in ruby, *Nature*, 1960, **187**, 493–494. https://www.nature.com/articles/187493a0.

5 R. D. Fonseca, M. G. Vivas, D. L. Silva, G. Eucat, Y. Bretonnière, C. Andraud, L. De Boni and C. R. Mendonça, First-Order Hyperpolarizability of Triphenylamine Derivatives Containing Cyanopyridine: Molecular Branching Effect, *J. Phys. Chem. C*, 2018, **122**, 1770–1778, DOI: 10.1021/acs.jpcc.7b05829.

6 P. S. Halasyamani and W. Zhang, Viewpoint: Inorganic Materials for UV and Deep-UV Nonlinear-Optical Applications, *Inorg. Chem.*, 2017, **56**, 12077–12085, DOI: 10.1021/acs.inorgchem.7b02184.

7 J. Deb, D. Paul and U. Sarkar, Density Functional Theory Investigation of Nonlinear Optical Properties of T-Graphene Quantum Dots, *J. Phys. Chem. A*, 2020, **124**, 1312–1320, DOI: 10.1021/acs.jpca.9b10241.

8 B. Mohan, M. Choudhary, S. Bharti, A. Jana, N. Das, S. Muhammad, A. G. Al-Sehemi and S. Kumar, Syntheses, characterizations, crystal structures and efficient NLO applications of new organic compounds bearing 2-methoxy-4-nitrobenzeneamine moiety and copper (II) complex of (E)-N'-(3, 5-dichloro-2-hydroxybenzylidene) benzohydrazide, *J. Mol. Struct.*, 2019, **1190**, 54–67. https://www.sciencedirect.com/science/article/pii/S0022286019304600.

9 L. M. Haupert and G. J. Simpson, Chirality in Nonlinear Optics, *Annu. Rev. Phys. Chem.*, 2009, **60**, 345–365, DOI: 10.1146/annurev.physchem.59.032607.093712.

10 P. Sałek, O. Vahtras, T. Helgaker and H. Ågren, Density-functional theory of linear and nonlinear time-dependent molecular properties, *J. Chem. Phys.*, 2002, **117**, 9630–9645. https://pubs.aip.org/aip/jcp/article-abstract/117/21/9630/451749.

11 S. Van Elshocht, T. Verbiest, M. Kauranen, A. P. Persoons, B. M. W. Langeveld-Voss and E. W. Meijer, Direct evidence of the failure of electric-dipole approximation in second-harmonic generation from a chiral polymer film, *J. Chem. Phys.*, 1997, **107**, 8201–8203. https://research.tue.nl/en/publications/direct-evidence-of-the-failure-of-electric-dipole-approximation-i.

12 A. Wojciechowski, M. M. M. Raposo, M. C. R. Castro, W. Kuznik, I. Fuks-Janczarek, M. Pokladko-Kowar and F. Bureš, Nonlinear optoelectronic materials formed by push–pull (bi) thiophene derivatives functionalized with di (tri) cyanovinyl acceptor groups, *J. Mater. Sci.: Mater. Electron.*, 2014, **25**, 1745–1750, DOI: 10.1007/s10854-014-1793-6.

13 N. Islam and A. H. Pandith, Optoelectronic and nonlinear optical properties of triarylamine helicenes: a DFT study, *J. Mol. Model.*, 2014, **20**, 1–17, DOI: 10.1007/s00894-014-2535-7.

14 D. S. Chemla, *Nonlinear Optical Properties of Organic Molecules and Crystals V1*, Elsevier, 2012.

15 M. Panneerselvam, A. Kathiravan, R. V. Solomon and M. Jaccob, The role of π-linkers in tuning the optoelectronic properties of triphenylamine derivatives for solar cell applications–A DFT/TDDFT study, *Phys. Chem. Chem. Phys.*, 2017, **19**, 6153–6163. https://pubs.rsc.org/en/content/articlehtml/2017/cp/c6cp07768d.

16 E. Appalanaidu, V. M. Vidya, M. R. Busireddy, J. R. Vaidya and P. Chetti, Effect of fluorine on optoelectronic properties in DI-A-DII-A-DI type organic molecules: A combined experimental and DFT study, *J. Mol. Struct.*, 2020, **1210**, 128019. https://www.sciencedirect.com/science/article/pii/S0022286020303446.

17 A. U. Hassan, A. Mohyuddin, C. Güleryüz, S. Nadeem, N. K. Nkungli, S. U. Hassan and M. Javed, Novel pull–push organic switches with D–π–A structural designs: computational design of star shape organic materials, *Struct. Chem.*, 2023, **34**, 399–412, DOI: 10.1007/s11224-022-01983-3.

18 M. SasiKumar, G. Maddala, M. Ambapuram, M. Subburu, J. R. Vaidya, S. N. Babu, P. Chetti, R. Mitty and S. Pola, Cost-effective thiophene-assisted novel dopant-free hole transport materials for efficient perovskite solar cell performance, *Sustainable Energy Fuels*, 2020, **4**, 4754–4767. https://pubs.rsc.org/en/content/articlehtml/2013/jk/d0se00549e.

19 K. S. Vishrutha, H. Ulla, B. R. Bhat and A. V. Adhikari, Utilization of newly configured carbazole-cyanopyridone structural hybrids towards achieving high-performance cyan fluorescent organic light-emitting diodes, *Mater. Adv.*, 2024, **5**, 2335–2346. https://pubs.rsc.org/en/content/articlehtml/2024/ma/d3ma00922j.

20 M. Yang, X. Tan, B. Yin, S. Kim, S. Pang, Z. Chen, X. Yang, C. Yang, Z. Liu and C. Duan, Near-Infrared Electron Acceptors with Cyano-Substituted 2-(3-Oxo-2,3-dihydroinden-1-ylidene)malononitrile End-Groups for Organic Solar Cells, *ACS Energy Lett.*, 2023, **8**, 2641–2651, DOI: 10.1021/acsenergylett.3c00664.

21 M. Khalid, I. Shafiq, M. A. Asghar, A. A. C. Braga, S. M. Alshehri, M. Haroon and M. L. Sanyang, Promising impact of push–pull configuration into designed octacyclic naphthalene-based organic scaffolds for nonlinear optical amplitudes: a quantum chemical approach, *Sci. Rep.*, 2023, **13**, 20104, DOI: 10.1038/s41598-023-44327-9.

22 N. Sahu, S. S. Khire and S. R. Gadre, Combining fragmentation method and high-performance computing: Geometry optimization and vibrational spectra of proteins, *J. Chem. Phys.*, 2023, **159**(4), DOI: 10.1063/5.0149572.

23 Y. Zhao and D. G. Truhlar, The M06 suite of density functionals for main group thermochemistry, thermochemical kinetics, noncovalent interactions, excited states, and transition elements: two new functionals and

© 2026 The Author(s). Published by the Royal Society of Chemistry

Open Access Article. Published on 08 May 2026. Downloaded on 5/10/2026 4:06:46 PM. This article is licensed under a Creative Commons Attribution-NonCommercial 3.0 Unported Licence.

systematic testing of four M06-class functionals and 12 other functionals, *Theor. Chem. Acc.*, 2008, **120**(1), 215–241.

24 M. D. Hanwell, D. E. Curtis, D. C. Lonie, T. Vandermeersch, E. Zurek and G. R. Hutchison, Avogadro: an advanced semantic chemical editor, visualization, and analysis platform, *J. Cheminf.*, 2012, **4**, 17, DOI: 10.1186/1758-2946-4-17.

25 A. Tenderholt, *PyMOlyze, Version 1.1*, Stanford University, Stanford, 2006, vol. 4, pp. 580–592.

26 N. M. O'boyle, A. L. Tenderholt and K. M. Langner, cclib: A library for package-independent computational chemistry algorithms, *J. Comput. Chem.*, 2008, **29**, 839–845, DOI: 10.1002/jcc.20823.

27 K. J. Stevenson, Review of originpro 8.5, *J. Am. Chem. Soc.*, 2011, **133**, 5621. https://www.originlab.com/pdfs/JACS_(Keith_Stevenson)_ja202216h.pdf.

28 E. D. Glendening, A. E. Reed, J. E. Carpenter and F. Weinhold, *Nbo Version 3.1, Tci*, University of Wisconsin, Madison, 1998, vol. 65.

29 J.-L. Oudar and D. S. Chemla, Hyperpolarizabilities of the nitroanilines and their relations to the excited state dipole moment, *J. Chem. Phys.*, 1977, **66**, 2664–2668. https://pubs.aip.org/aip/jcp/article-abstract/66/6/2664/89594.

30 A. Alparone, Linear and nonlinear optical properties of nucleic acid bases, *Chem. Phys.*, 2013, **410**, 90–98. https://www.sciencedirect.com/science/article/pii/S0301010412004338.

31 A. Plaquet, M. Guillaume, B. Champagne, F. Castet, L. Ducasse, J.-L. Pozzo and V. Rodriguez, In silico optimization of merocyanine-spiropyran compounds as second-order nonlinear optical molecular switches, *Phys. Chem. Chem. Phys.*, 2008, **10**, 6223–6232. https://pubs.rsc.org/en/content/articlehtml/2008/cp/b806561f.

32 S.-L. Chang, K.-E. Hung, F.-Y. Cao, K.-H. Huang, C.-S. Hsu, C.-Y. Liao, C.-H. Lee and Y.-J. Cheng, Isomerically Pure Benzothiophene-Incorporated Acceptor: Achieving Improved V_{oc} and J_{sc} of Nonfullerene Organic Solar Cells via End Group Manipulation, *ACS Appl. Mater. Interfaces*, 2019, **11**, 33179–33187, DOI: 10.1021/acsami.9b08462.

33 T. Lu and F. Chen, Multiwfn: A Multifunctional Wavefunction Analyzer, *J. Comput. Chem.*, 2012, **33**, 580–592.

34 M. U. Saeed, N. Hadia, J. Iqbal, M. Hessien, A. M. Shawky, M. Ans, N. S. Alatawi and R. A. Khera, Impact of End-Group Modifications and Planarity on Bdp-Based Non-Fullerene Acceptors for High-Performance Organic Solar Cells by Using Dft Approach, *J. Mol. Model.*, 2022, **28**, 397.

35 M. U. Khan, R. Hussain, M. Yasir Mehboob, M. Khalid, Z. Shafiq, M. Aslam, A. A. Al-Saadi, S. Jamil and M. R. S. A. Janjua, In Silico Modeling of New "Y-Series"-Based Near-Infrared Sensitive Non-Fullerene Acceptors for Efficient Organic Solar Cells, *ACS Omega*, 2020, **5**, 24125–24137, DOI: 10.1021/acsomega.0c03796.

36 A. Ramalingam, S. Sambandam, M. Medimagh, O. Al-Dossary, N. Issaoui and M. J. Wojcik, Study of a new piperidone as an anti-Alzheimer agent: Molecular docking, electronic and intermolecular interaction investigations by DFT method, *J. King Saud Univ. Sci.*, 2021, **33**, 101632. https://www.sciencedirect.com/science/article/pii/S1018364721002949.

37 R. Arulraj, Hirshfeld surface analysis, interaction energy calculation and spectroscopical study of 3-chloro-3-methyl-r (2), c (6)-bis (p-tolyl) piperidin-4-one using DFT approaches, *J. Mol. Struct.*, 2022, **1248**, 131483. https://www.sciencedirect.com/science/article/pii/S0022286021016112.

38 R. Rahmani, N. Boukabcha, A. Chouaih, F. Hamzaoui and S. Goumri-Said, On the molecular structure, vibrational spectra, HOMO-LUMO, molecular electrostatic potential, UV–Vis, first order hyperpolarizability, and thermodynamic investigations of 3-(4-chlorophenyl)-1-(1yridine-3-yl) prop-2-en-1-one by quantum chemistry calculations, *J. Mol. Struct.*, 2018, **1155**, 484–495. https://www.sciencedirect.com/science/article/pii/S0022286017315065.

39 M. Arivazhagan and S. Jeyavijayan, Vibrational spectroscopic, first-order hyperpolarizability and HOMO, LUMO studies of 1, 2-dichloro-4-nitrobenzene based on Hartree–Fock and DFT calculations, *Spectrochim. Acta, Part A*, 2011, **79**, 376–383. https://www.sciencedirect.com/science/article/pii/S1386142511001995.

40 M. Arivazhagan and G. Thilagavathi, Vibrational study, first hyperpolarizability and HOMO–LUMO analyses on the structure of 2-hydroxy-6-nitro toluene, *Spectrochim. Acta, Part A*, 2012, **91**, 411–418. https://www.sciencedirect.com/science/article/pii/S1386142512001291.

41 V. Balachandran, A. Nataraj and T. Karthick, Molecular structure, spectroscopic (FT-IR, FT-Raman) studies and first-order molecular hyperpolarizabilities, HOMO–LUMO, NBO analysis of 2-hydroxy-p-toluic acid, *Spectrochim. Acta, Part A*, 2013, **104**, 114–129. https://www.sciencedirect.com/science/article/pii/S1386142512011481.

42 M. Akram, M. Adeel, M. Khalid, M. N. Tahir, M. U. Khan, M. A. Asghar, M. A. Ullah and M. Iqbal, A combined experimental and computational study of 3-bromo-5-(2, 5-difluorophenyl) pyridine and 3, 5-bis (naphthalen-1-yl) pyridine: Insight into the synthesis, spectroscopic, single crystal XRD, electronic, nonlinear optical and biological properties, *J. Mol. Struct.*, 2018, **1160**, 129–141. https://www.sciencedirect.com/science/article/pii/S002228601830139X.

43 S. Uzun, Z. Esen, E. Koç, N. C. Usta and M. Ceylan, Experimental and density functional theory (MEP, FMO, NLO, Fukui functions) and antibacterial activity studies on 2-amino-4-(4-nitrophenyl)-5, 6-dihydrobenzo [h] quinoline-3-carbonitrile, *J. Mol. Struct.*, 2019, **1178**, 450–457. https://www.sciencedirect.com/science/article/pii/S0022286018311785.

44 M. Khalid, I. Shafiq, M. Zhu, M. U. Khan, Z. Shafiq, J. Iqbal, M. M. Alam, A. A. C. Braga and M. Imran, Efficient tuning of small acceptor chromophores with A1-π-A2-π-A1 configuration for high efficacy of organic solar cells via end group manipulation, *J. Saudi Chem. Soc.*, 2021, **25**, 101305. https://www.sciencedirect.com/science/article/pii/S1319610321001101.

Open Access Article. Published on 08 May 2026. Downloaded on 5/10/2026 4:06:46 PM. This article is licensed under a Creative Commons Attribution-NonCommercial 3.0 Unported Licence.

45 R. G. Parr and W. Yang, Density functional approach to the frontier-electron theory of chemical reactivity, *J. Am. Chem. Soc.*, 1984, **106**, 4049–4050, DOI: 10.1021/ja00326a036.

46 R. G. Parr, R. A. Donnelly, M. Levy and W. E. Palke, Electronegativity: the density functional viewpoint, *J. Chem. Phys.*, 1978, **68**, 3801–3807. https://pubs.aip.org/aip/jcp/article-abstract/68/8/3801/789300.

47 P. Politzer and D. G. Truhlar, Introduction: The Role of the Electrostatic Potential in Chemistry, in *Chemical Applications of Atomic and Molecular Electrostatic Potentials*, ed. P. Politzer and D. G. Truhlar, Springer US, Boston, MA, 1981, pp. 1–6, DOI: 10.1007/978-1-4757-9634-6_1.

48 R. G. Parr and R. G. Pearson, Absolute hardness: companion parameter to absolute electronegativity, *J. Am. Chem. Soc.*, 1983, **105**, 7512–7516, DOI: 10.1021/ja00364a005.

49 R. G. Pearson, Absolute electronegativity and absolute hardness of Lewis acids and bases, *J. Am. Chem. Soc.*, 1985, **107**, 6801–6806, DOI: 10.1021/ja00310a009.

50 R. Parthasarathi, J. Padmanabhan, M. Elango, V. Subramanian and P. K. Chattaraj, Intermolecular reactivity through the generalized philicity concept, *Chem. Phys. Lett.*, 2004, **394**, 225–230. https://www.sciencedirect.com/science/article/pii/S0009261404010164.

51 M. Khalid, I. Shafiq, K. Mahmood, R. Hussain, M. F. Ur Rehman, M. A. Assiri, M. Imran and M. S. Akram, Effect of different end-capped donor moieties on non-fullerenes based non-covalently fused-ring derivatives for achieving high-performance NLO properties, *Sci. Rep.*, 2023, **13**, 1395. https://www.nature.com/articles/s41598-023-28118-w.

52 M. Khalid, S. Murtaza, K. Gull, S. Abid, M. Imran and A. A. C. Braga, Influence of acceptors on the optical nonlinearity of 5 H -4-oxa-1,6,9-trithia-cyclopenta[b]-as-indacene-based chromophores with a push–pull assembly: a DFT approach, *RSC Adv.*, 2024, **14**, 1169–1185, DOI: 10.1039/D3RA06673H.

53 P. Goszczycki, K. Stadnicka, M. Z. Brela, J. Grolik and K. Ostrowska, Synthesis, crystal structures, and optical properties of the π-π interacting pyrrolo [2, 3-b] quinoxaline derivatives containing 2-thienyl substituent, *J. Mol. Struct.*, 2017, **1146**, 337–346. https://www.sciencedirect.com/science/article/pii/S0022286017307846.

54 Liu, An sp-hybridized all-carboatomic ring, cyclo… – Google Scholar, https://scholar.google.com/scholar_lookup?title=Ansp-hybridizedall-carboatomicring%2Ccyclo18carbon%3AElectronicstructure%2Celectronicspectrum%2Candopticalnonlinearity&publication_year=2020&author=Z.Liu&author=T.Lu&author=Q.Chen (accessed July 7, 2025).

55 Chandralekha: Quantum mechanical, spectroscopic and… – Google Scholar, https://scholar.google.com/scholar_lookup?&title=&journal=Chem.DataCollect.&doi=10.1016%2Fj.cdc.2019.100183&volume=19&publication_year=2019&author=Chandralekha%2CB&author=Hemamalini Rajagopal%2CS&author=Muthu%2CS (accessed July 3, 2025).

56 J. A. Agwupuye, H. Louis, T. O. Unimuke, P. David, E. I. Ubana and Y. L. Moshood, Electronic structure investigation of the stability, reactivity, NBO analysis, thermodynamics, and the nature of the interactions in methyl-substituted imidazolium-based ionic liquids, *J. Mol. Liq.*, 2021, **337**, 116458. https://www.sciencedirect.com/science/article/pii/S016773222101182X.

57 C. Xu, K. Jin, Z. Xiao, Z. Zhao, Y. Yan, X. Zhu, X. Li, Z. Zhou, S. Y. Jeong, L. Ding, H. Y. Woo, G. Yuan and F. Zhang, Efficient Semitransparent Layer-by-Layer Organic Photovoltaics via Optimizing Wide Bandgap and Narrow Absorption Polymer Layer Thickness, *Sol. RRL*, 2022, **6**, 2200308, DOI: 10.1002/solr.202200308.

58 B. S. Mendis and K. N. De Silva, A comprehensive study of linear and non-linear optical properties of novel charge transfer molecular systems, *J. Mol. Struct.: THEOCHEM*, 2004, **678**, 31–38. https://www.sciencedirect.com/science/article/pii/S0166128004001393.

59 S. Muhammad, R. A. Shehzad, J. Iqbal, A. G. Al-Sehemi, M. Saravanabhavan and M. Khalid, Benchmark study of the linear and nonlinear optical polarizabilities in prototype NLO molecule of para-nitroaniline, *J. Theor. Comput. Chem.*, 2019, **18**(06), 1950030.

© 2026 The Author(s). Published by the Royal Society of Chemistry